Analyses and modeling of evolving turbulent flow

By P. A. Durbin

Work done during this year includes: an asymptotic analysis of adverse pressure gradient boundary layers (Durbin and Belcher 1991); a rapid-distortion analysis of homogeneous, compressed turbulence and formulation of a new pressure-dilatation model therefrom (Durbin and Zeman 1991); and refinement of the $k-\varepsilon-v$ near-wall model (Durbin 1990), with extension to calculations of heat transfer.

1. Motivation and objectives

The ultimate motivation for this work is the development of analytical models for turbulence statistics. The approach which I have adopted is to attempt to use theoretical results as guidance for model development. For example, in last year's report (Durbin 1990), I described a near wall model which was motivated by analyses of kinematic blocking; in section 4 of the present report I will describe further computations with that model. These consist of calculations of the turbulent flat-plate boundary layer, including heat transfer, and of heat transfer calculations for channel flow. The calculations are compared to experimental and DNS data. This work on near-wall turbulence modeling is still in progress; Dr. S. Ko is incorporating the model into an elliptic code, so that more complex flows can be computed (see Ko's article in this volume).

In anticipation of future computational work and modeling of more complex boundary-layer type flows, an asymptotic analysis was done of the structure of strongly adverse pressure gradient (APG) turbulent boundary layers. This was motivated by previous asymptotic analyses of zero pressure gradient (ZPG) boundary layers (Mellor 1973) and the semi-empirical observation (Townsend 1976) that the adverse pressure gradient boundary layer has a $y^{1/2}$ region, where y is distance from the surface. At the outset, it was supposed that the two region (wall and wake) ZPG scaling could be modified so that a $y^{1/2}$-law would replace the logarithmic overlap law. However, the half-power law did not permit a proper overlap of wall and wake regions; a third, intermediate region seems to be required (see fig. 1). The results of this investigation are summarized in section 2 and in Belcher's article in this volume.

As a result of discussions with Gary Coleman and Otto Zeman, I felt that a rapid-distortion analysis of homogeneously compressed turbulence might help to gain an understanding of some effects that occur in compressible flows. In particular, of the pressure-dilatation term in the turbulent kinetic energy equation, which would seem to be important in flows with shock waves or in compression corners or pistons (Zeman 1991). A rapid distortion analysis for the small turbulent Mach number limit is described in section 3. It is shown how the magnitude of pressure-dilatation correlation depends on the symmetry of the compression, vanishing for spherical

symmetry and increasing with asymmetry. The RDT analysis and invariant closure modeling suggest a model for pressure-dilatation; that model will be discussed briefly.

2. Asymptotic scaling of adverse pressure-gradient boundary layers

Because of the summary nature of the present report, the reader is referred to Durbin and Belcher (1991) for details. We consider a uniform density, incompressible turbulent boundary layer subject to a strong adverse pressure gradient (APG). The free-stream mean velocity is $U_\infty(x)$. The kinematic pressure-gradient, denoted by α, a streamwise length scale L, and viscous pressure-gradient velocity u_p are defined by

$$\alpha \equiv -U_\infty U_{\infty_x}\,;\; L \equiv U_\infty^2/\alpha\,;\; u_p \equiv (\nu\alpha)^{1/3}\,. \tag{1}$$

The definition of u_p reflects the fact that the relevant dimensional parameters near the wall are ν and α. The small parameter in the present analysis is

$$\epsilon \equiv u_p/U_\infty = \left(\nu\alpha/U_\infty^3\right)^{1/3} = R_L^{-1/3} \tag{2}$$

where R_L is the Reynolds number based on L. δ denotes a scale for the boundary layer thickness. It is sufficient (although not necessary) to let $\delta/L \sim \epsilon$; this gives the appropriate leading order balance between pressure gradient and turbulent shear-stress gradient in the middle and outer regions. Given this ordering, one can define δ such that this latter relation is an equality. In most of the analysis, it is appropriate to think of δ/L as the small parameter. The middle and outer regions are inviscid to lowest order, so it would be misleading to associate the small parameter with Reynolds number in these regions; perhaps (2) should be expressed as $R_L = \epsilon^{-3}$.

The three asymptotic regions of an APG turbulent boundary layer reflect three velocity scales which exist in such a flow. They are: the viscous, pressure-gradient velocity, u_p; the free-stream velocity, U_∞; and $\sqrt{\alpha\delta}$. The first is used to non-dimensionalize the mean velocity in the wall region, the second nondimensionalizes the wake region, and the last nondimensionalizes the middle region. Another velocity scale is the friction velocity, u_*. In the present analysis this is taken to be of the same order as u_p. The three regions and their scaling are shown schematically by figure 1.

Scaling of the regions

The thickness of the inner region is ν/u_p, or $\epsilon^2 L$. Here the leading order balance is between pressure gradient, viscous, and turbulent stresses. The mean momentum equation, in non-dimensional form, becomes

$$\left((1+\hat{\nu}_t)\hat{U}_{\hat{y}}\right)_{\hat{y}} = 1 + O(\epsilon^2) \tag{3}$$

where $\hat{U} = U/u_p$, $\hat{\nu}_t = \nu_t/\nu$ is the turbulent eddy viscosity, and $\hat{y} = yu_p/\nu$.

In the middle region, the leading order balance is between pressure gradient and turbulent stress. The precise scaling depends on how the turbulent stress is modeled.

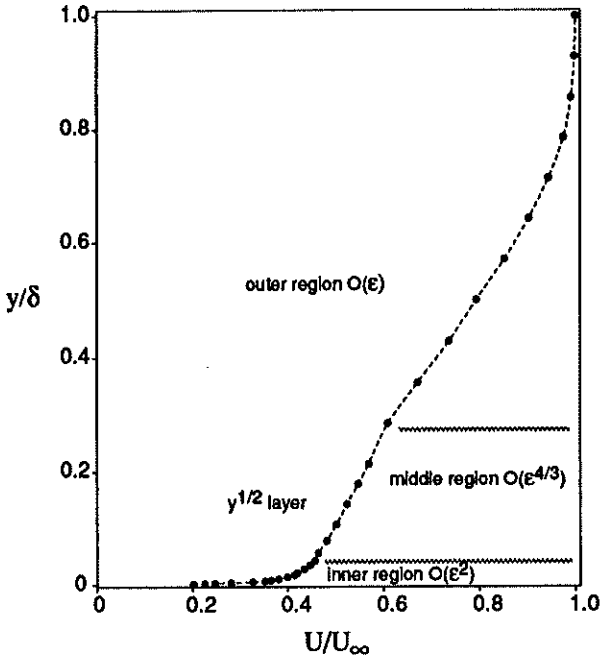

FIGURE 1. Schematic of structure of APG boundary layers. The experimental data is from Bradshaw and Ferris (Coles and Hirst 1968).

In general, the thickness of the middle region is $O(\epsilon^n L)$ where $1 < n < 2$. If the eddy viscosity is constant in the outer region, then $n = 4/3$, which is the case described here. The mean momentum equation simplifies to

$$\left(\bar{\nu}_t \bar{U}_{\tilde{y}}\right)_{\tilde{y}} = 1 + O(\epsilon^{4/3}). \tag{4}$$

where $\bar{U} = U/U_\infty \epsilon^{3/2}$, and $\bar{\nu}_t = \nu_t/U_\infty \delta \epsilon$.

The outer region balance is between pressure gradient, turbulent stress, and inertia. The mean momentum equation becomes

$$\tilde{U}\tilde{U}_{\tilde{x}} + \tilde{V}\tilde{U}_{\tilde{y}} - \tilde{y}\tilde{U}\tilde{U}_{\tilde{y}}\frac{\delta_{\tilde{x}}}{\delta} - \tilde{U}^2 + 1 = \left(\tilde{\nu}_t \tilde{U}_{\tilde{y}}\right)_{\tilde{y}} + O(\epsilon^2) \tag{5}$$

in the outer, wake region. Here $\tilde{U} = U/U_\infty$, $\tilde{y} = y/\delta$, $\tilde{V} = V/U_\infty \epsilon$, $\tilde{\nu}_t = \nu_t/U_\infty \delta \epsilon$ and $d\tilde{x} = dx/L$. V is determined by the continuity equation, which can be written

$$\tilde{U}_{\tilde{x}} + \tilde{V}_{\tilde{y}} - \tilde{U} - \frac{\delta_{\tilde{x}}}{\delta}\tilde{y}\tilde{U}_{\tilde{y}} = 0. \tag{6}$$

In (5) and (6) an $\tilde{x}$ dependence of U_∞ and δ has been allowed; this dependence is required in the self-similar solution cited below.

The half-power law describes the overlap layer between the inner and middle regions. It exists because of the linear variation of shear stress in a strong APG boundary layer: $\tau = \alpha y + u_*^2$. The half power can be derived when $y >> u_*^2/\alpha$ from a mixing length argument (Townsend 1976). However, because of its relevance to closure modeling, I will note here that the standard $k-\varepsilon$ model has the solution

$$\hat{U} = A_u y^{1/2} \tag{7}$$

with

$$A_u^4 = \frac{4(\sigma_k - 3C_{\varepsilon_1}\sigma_\varepsilon)(\sigma_k - 3C_{\varepsilon_2}\sigma_\varepsilon)}{C_\mu \sigma_k^2 \sigma_\varepsilon^2 (C_{\varepsilon_2} - C_{\varepsilon_1})^2}$$

in a linear stress layer. With the commonly used values,

$$C_{\varepsilon_1} = 1.44;\ C_{\varepsilon_2} = 1.92;\ C_\mu = 0.09;\ \sigma_k = 1.0;\ \sigma_\varepsilon = 1.3$$

this gives $A_u = 7.65$.

Self-similar solution

The problem posed by (3)-(6) must be solved subject to $U = 0$ at $y = 0$ and $U \to U_\infty$ as $y \to \infty$. In an asymptotic framework, such a solution requires formal matching between the regions. With the present eddy-viscosity representation for the turbulent shear stress, it also requires a prescription for ν_t. Omitting details, which can be found in Durbin and Belcher (1991), the analysis reduces to solving (5) and (6), with the Clauser viscosity $\tilde{\nu}_t = C_c \tilde{\delta}_*$, subject to the conditions

$$\tilde{U}(0) = \epsilon \hat{C}_u,\ \tilde{U}_y(0) = \epsilon^{2/3}\bar{C}_u + \epsilon u_*^2/(u_p^2 \tilde{\nu}_t),\ \tilde{V}(0) = \epsilon \bar{C}_v \tag{8}$$

and $\tilde{U} \to 1$ as $\tilde{y} \to \infty$. $\hat{C}_u$, $\bar{C}_u$ and $\bar{C}_v$ are constants determined by the inner and middle region solutions. They are given by equation (4.26) of Durbin and Belcher (1991) for the eddy viscosity formulation adopted in that paper.

For a self-similar boundary layer, the pressure gradient enters through the parameter

$$\beta = -U_\infty \frac{d\delta}{dx} \Big/ \delta \frac{dU_\infty}{dx}$$

which appears in the self-similar version of (5). For the power law $U_\infty \propto x^{-a}$ and a linearly growing boundary layer thickness, $\beta = 1/a$. Figure 2 shows a computation of normalized friction velocity, u_*/u_p versus β. This figure shows an interesting property of the analysis: the skin friction is a double valued function of pressure gradient. In figure 2, this occurs in a small range near $\beta = 4.8$. Thus, for a given pressure gradient, two self-similar boundary layers exist: one with small skin friction, for which the downstream increase of the momentum thickness is largely balanced by pressure gradient; and one with larger skin friction, for which the growth of momentum thickness is largely balanced by skin friction. These double valued boundary layers have been observed experimentally by Clauser (1954). Further results of the analysis can be found in Belcher's article.

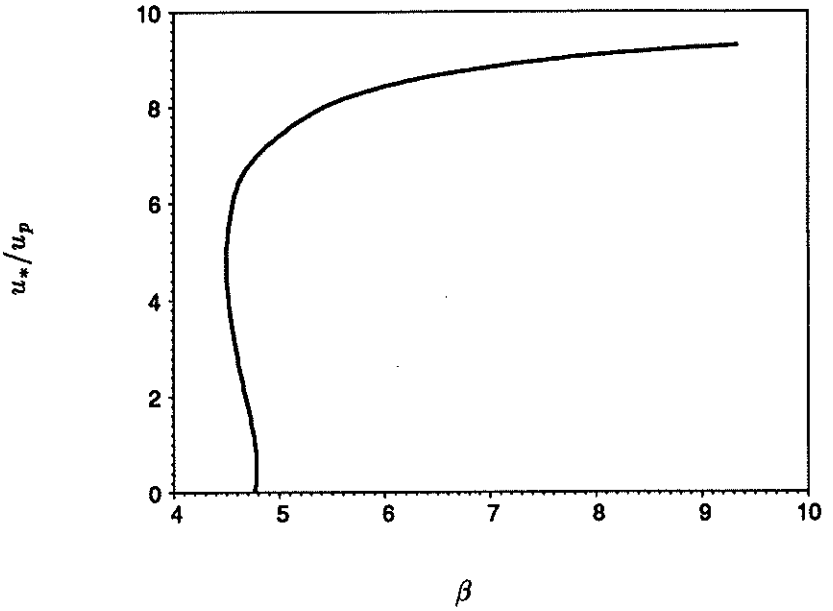

FIGURE 2. Friction velocity versus pressure gradient parameter for self-similar APG boundary layer.

3. Rapid distortion theory for compressed homogeneous turbulence

An RDT analysis of compressed homogeneous turbulence was undertaken in conjunction with research in progress at CTR on simulation and modeling of compressible homogeneous turbulence (Coleman and Mansour 1991, Zeman 1991). The method of analysis is not novel; the motivation was to gain an understanding of and to model the pressure-dilatation term in the turbulent kinetic energy equation.

Analysis

RDT analysis is based on the assumption that the time-scale for distortion by mean strain is short compared to that for self-distortion of the turbulent eddies (Hunt 1973). Linearized equations are solved for the evolution of the turbulence from an initially isotropic state.

The requirement for homogeneity is that the mean pressure, density, and velocity gradient be uniform in space. Thus, the mean velocity is of the form $\mathbf{U} = \mathbf{x} \cdot \mathbf{S}(t)$. An irrotational mean flow is considered. In a principle-axes coordinate system, the mean momentum equation requires $\mathbf{S}$ to have the time dependence

$$\mathbf{S} = \begin{pmatrix} a_1/(1+a_1 t) & 0 & 0 \\ 0 & a_2/(1+a_2 t) & 0 \\ 0 & 0 & a_3/(1+a_3 t) \end{pmatrix} \tag{9}$$

where the a_i's are arbitrary constants. To facilitate this discussion of the RDT

solution, we introduce the matrix of material line distortions

$$\mathbf{J} = \begin{pmatrix} 1/(1+a_1 t) & 0 & 0 \\ 0 & 1/(1+a_2 t) & 0 \\ 0 & 0 & 1/(1+a_3 t) \end{pmatrix}. \tag{10}$$

Given that ρ is spatially uniform and that $D\mathbf{U}/Dt = 0$ and $D\rho/Dt = -\rho\nabla\cdot\mathbf{U}$, the linearized, inviscid fluctuating momentum, continuity, and entropy equations can be written (Goldstein 1978)

$$\begin{aligned} \rho(Du'/Dt + u'\cdot\nabla U) &= -\nabla p' \\ D(\rho'/\rho)/Dt &= -\nabla\cdot u' \\ Ds'/Dt &= 0. \end{aligned} \tag{11}$$

An important relation between pressure-dilatation and pressure variance follows from (11):

$$\overline{p'\nabla\cdot u'} = -\frac{1}{2}\gamma P\frac{d}{dt}\left(\frac{\overline{p'^2}}{(\gamma P)^2}\right) \tag{12}$$

where γ is the ratio of specific heats. Our primary results and new developments on closure modeling derive from (12). Although the equation for entropy fluctuations is included in (11), because the mean pressure is uniform, vortical fluctuations cannot be produced from entropy fluctuations in homogeneous turbulence.

In general, the solution to (11) is facilitated by Goldstein's (1978) decomposition of the fluctuating velocity into irrotational and vortical parts. However, for the special case of homogeneous turbulence, the Helmholtz decomposition into irrotational and solenoidal parts can be used. We first introduce a Fourier representation (Hunt 1973):

$$\mathbf{u}' = \int_{-\infty}^{\infty} \hat{\mathbf{u}} e^{i\mathbf{k}(t)\cdot\mathbf{x}}\, d^3\mathbf{k}_0$$

in which $\mathbf{k}(t) = \mathbf{k}_0\cdot\mathbf{J}$. Then the Helmholtz decomposition can be written

$$\hat{\mathbf{u}} = \left[\hat{\mathbf{u}}_0\cdot\mathbf{J} - \frac{\mathbf{k}\mathbf{k}\cdot\hat{\mathbf{u}}_0\cdot\mathbf{J}}{|\mathbf{k}|^2}\right] + i\mathbf{k}\phi \tag{13}$$

where the bracketed term is the solenoidal component—that is, it is orthogonal to $\mathbf{k}$. $\hat{\mathbf{u}}_0$ is the initial solenoidal velocity. In consequence of (11), ϕ satisfies

$$\frac{d}{dt}(c^{-2}\frac{d\phi}{dt}) + |\mathbf{k}|^2\phi = -i\frac{d}{dt}\left(c^{-2}\frac{d}{dt}\frac{\mathbf{k}\cdot\hat{\mathbf{u}}_0\cdot\mathbf{J}}{|\mathbf{k}|^2}\right). \tag{14}$$

ϕ is the only quantity for which an equation has to be solved.

The details of the analysis can be found in Durbin and Zeman (1991). Here, we simply note that when the fluctuating Mach number is small, the right side of (14) can be neglected to lowest order of approximation. Then the solenoidal and

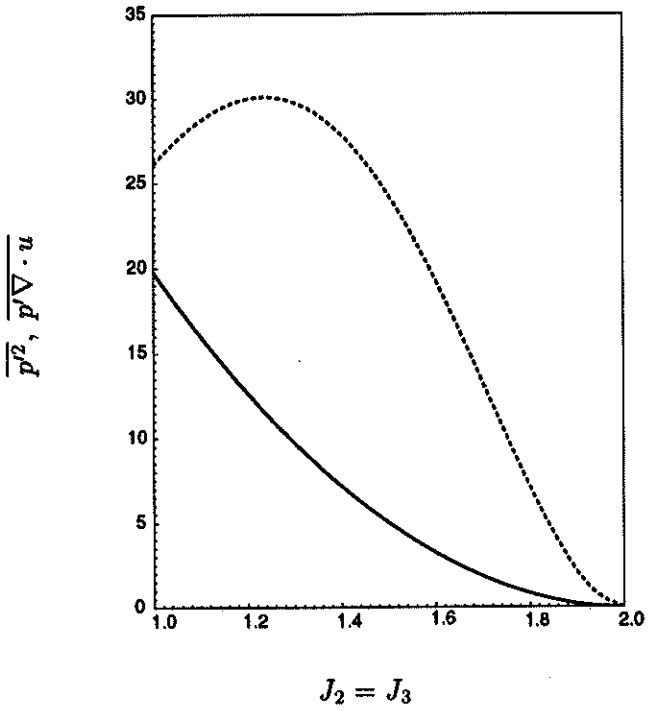

FIGURE 3. Solenoidal contribution to pressure variance and pressure dilatation for axisymmetric compression with $J_1 = 2$ and $J_2 = J_3$. Solid line is $\overline{p'^2}$ dashed line is $\overline{p'\nabla \cdot u}$.

irrotational (acoustic) components decouple. Correspondingly, the pressure can be separated into an acoustic component and a solenoidal component. The solution for the solenoidal pressure works out to be

$$\overline{p'^2} = \frac{3q_0^2 L_0^2 \rho^2}{2\pi} \int_0^{2\pi} \int_0^{\pi} \frac{1}{(\mathbf{e}\cdot\mathbf{J^2}\cdot\mathbf{e})^2} \times$$

$$\left[(\mathbf{e}\cdot\mathcal{S}^2\cdot\mathbf{e}) - 2\frac{(\mathbf{e}\cdot\mathcal{S}\cdot\mathbf{e})(\mathbf{e}\cdot\mathcal{S}\cdot\mathbf{J^2}\cdot\mathbf{e})}{\mathbf{e}\cdot\mathbf{J^2}\cdot\mathbf{e}} + \frac{(\mathbf{e}\cdot\mathcal{S}\cdot\mathbf{e})^2(\mathbf{e}\cdot\mathbf{J^4}\cdot\mathbf{e})}{(\mathbf{e}\cdot\mathbf{J^2}\cdot\mathbf{e})^2}\right] \sin\theta d\theta d\phi \tag{15}$$

where $\mathbf{e} = (\cos\theta, \sin\theta\sin\phi, \sin\theta\cos\phi)$ and q_0 and L_0 are initial velocity and length scales, and in which $\mathcal{S} = \mathbf{J}\cdot\mathbf{S}\cdot\mathbf{J}$. After evaluation of (15), the pressure-dilatation is determined by (12). For axisymmetric compression, the integrals in (15) can be found in closed form.

Figure 3 shows results for the solenoidal component in an axi-symmetric compression. The J_i's denote the diagonal components of $\mathbf{J}$ in equation (10). When $J_2 = J_3 = 2$, the compression is spherically symmetric and the pressure variance

vanishes. The pressure-dilatation increases monotonically as J_2 decreases toward 1; hence, pressure-dilatation increases with increased asymmetry of the compression. DNS by Coleman and Mansour (1991 and Coleman private communication) show that pressure dilatation is very much larger for one-dimensional compression ($J_2 = 1$) than for spherically symmetric compression ($J_2 = 2$). Hence, the RDT results are in accord with DNS.

Modeling

The success of the RDT analysis suggests that (12) might be made the basis of a closure model; all that is required is an expression to substitute for $\overline{p'^2}$ on the right side. Of course, this equation is only complete when the distortion is rapid; more generally, non-linear terms cannot be ignored. However, the pressure-dilatation term in the turbulent kinetic energy equation is only important when the turbulence is subject to a rapid change—produced, *e. g.*, by a shock wave or by compression inside a cylinder—hence, the linearized formula might cover many practical cases.

Attention is again restricted to low fluctuation Mach number so that the solenoidal and acoustic contributions can be decoupled. Zeman (1991) has proposed an equation for the acoustic contribution to $\overline{p^2}$ which was adopted here. The solenoidal contribution can be modeled by making use of standard invariance and symmetry constraints (Lumley 1978). If the solenoidal pressure is expanded about isotropy, keeping only the first order terms in anisotropy, one finds that

$$\overline{p_s'^2} = (\rho q L)^2 \left[C_1 \mathrm{Tr}(\mathbf{S}_*^2) + C_2 b_{ij} S_{*_{ij}}^2 \right] + O(\|\mathbf{b}\|^2) \tag{16}$$

where $b_{ij} = \overline{u_i u_j}/q^2 - \delta_{ij}$ is the anisotropy tensor; $q^2 = \overline{u_i u_i}/3$ is the turbulent intensity; L is a length scale; and $S_{*_{ij}} = S_{ij} - \delta_{ij}\mathrm{Tr}(\mathbf{S})/3$ is the trace-free part of $\mathbf{S}$. Equations (12) and (16) were incorporated into a model described in Zeman (1991). That model contains an equation for L which accounts for the effect of compression on the length scale. Values for the constants C_1 and C_2 in (16) were obtained by requiring (16) to agree with the RDT solution at short times. This gives $C_1 = 6/5$ and $C_2 = 18/7$.

Figure 4 shows a model computation compared to data provided by Gary Coleman. The compression is one-dimensional, and the horizontal axis, τ, is a nondimensional time, related to compression ratio by $J_1 = 1/(1-\tau)$. The curve labelled $-\Pi_d$ is the pressure-dilatation. The rate of energy dissipation is not shown because it is extremely small in this computation of raid compression; the dominant balance in the turbulent kinetic energy equation is between production, pressure-dilatation, and rate of growth. The agreement between model and data is satisfactory and suggests that (12) and (16) are a viable approach. The effects of non-homogeneity and, at higher turbulent Mach number, the coupling between acoustic and solenoidal components would have to be included in a more general model.

4. The $k - \varepsilon - v$ model for boundary layer flow and heat transfer

The $k - \epsilon - v$ near-wall turbulence model was described in last year's report (Durbin 1990). Progress on further development and application of the model has

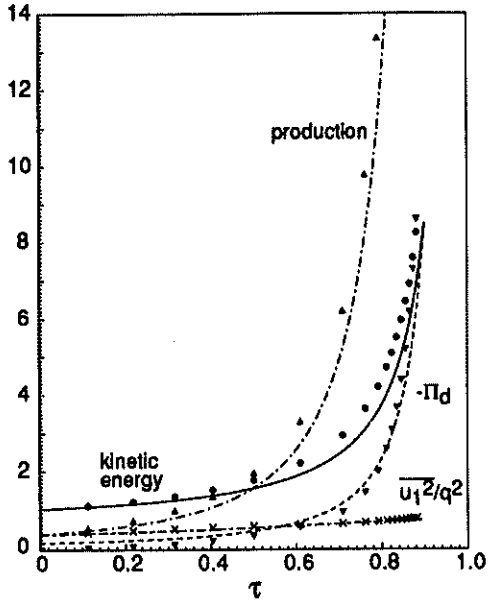

FIGURE 4. Comparison of model (lines) to DNS data (symbols) for rapid one-dimensional compression (case c1db of Coleman and Mansour 1991). τ is a non-dimensional time.

been a bit slower that expected. Here I will present results for flat plate boundary layers and for heat transfer in channel flow.

Refinements for boundary layer computation

The 'refinements' referred to in this subsection heading are small adjustments in the model constants, no alterations to the equations were made. The model was originally developed by making use of channel flow DNS data. Because this is a very simple flow, the model constants could be set fairly coarsely. In the boundary layer, the need to predict the growth rate of the thickness requires more refined values of the constants. I have also tried to bring the constants into line with values used by other modelers. For example, the ε-equation constants C_{ε_1} and C_{ε_2} were previously set to the round numbers 1.5 and 2. They have now been set to more conventional values of 1.44 and 1.9. (It should be noted that an important quantity is the *difference* between these constants; also, my ε-equation contains a 'local anisotropy' term (Durbin 1990), so that C_{ε_1} has a slightly non-conventional meaning.) I have also changed C_μ from 0.2 to 0.23; Launder (1989) uses 0.22.

The channel flow was recomputed and the agreement to DNS data was unchanged (see figures in Durbin 1990), with one caveat. The 'Prandtl numbers' σ_k and σ_ε were left at their previous values of 1.3 and 1.6 (Durbin 1991). These values were

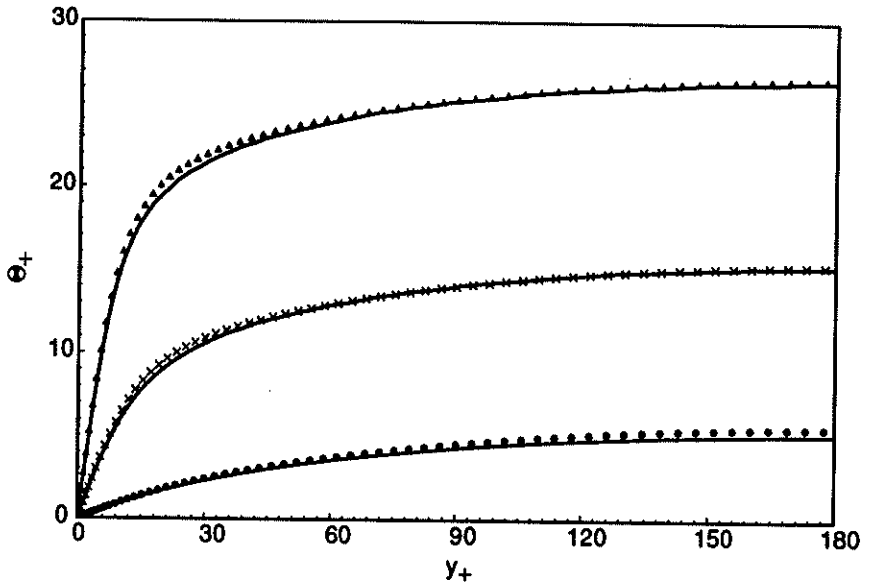

FIGURE 5. Model (lines) and DNS (symbols; Kim and Moin 1989) temperature profiles for turbulent channel flow at three molecular Prandtl numbers: $R_\tau = 180$. $\triangle$, $Pr = 2.0$, $\times$, $Pr = 0.71$, $\bullet$, $Pr = 0.1$.

obtained by requiring the centerline turbulent intensity to agree with the DNS data (at $Re_\tau = 395$). Because a boundary layer has a free-stream interface across which irrotational fluid is entrained, the transport of kinetic energy to the edge of the boundary layer is greater than in a channel flow; hence, the above Prandtl numbers had to be lower for the boundary layer computation—$\sigma_k = 0.9$ and $\sigma_\epsilon = 1.3$ were used, which are in line with values widely used for flows with a free stream (Launder, 1989, uses 1.0 and 1.3). The fact that different values of σ_k and σ_ϵ are required for enclosed and unbounded flows indicates that an aspect of the fluid mechanics (the irrotational-rotational interface) is not being represented by the differential equations of the model, and must be incorporated through the constants. This statement applies to other models, such as $k - \varepsilon$, and is not a peculiarity of the present model.

The mean temperature equation

$$U \cdot \nabla \Theta = -\partial_y(\overline{v\theta'} - \alpha \partial_y \Theta) \tag{17}$$

was included in the model to compute heat transfer. In most computations, $-\overline{v\theta'}$ was represented by the eddy diffusion formula $\alpha_t \partial_y \Theta$, with turbulent diffusivity determined by

$$Pr_t \alpha_t = \nu_t = C_\mu \overline{v^2} T \tag{18}$$

where Pr_t is the turbulent Prandtl number for heat transport. Temperature profiles for channel flow were also computed with a $\overline{v\theta'}$ differential equation.

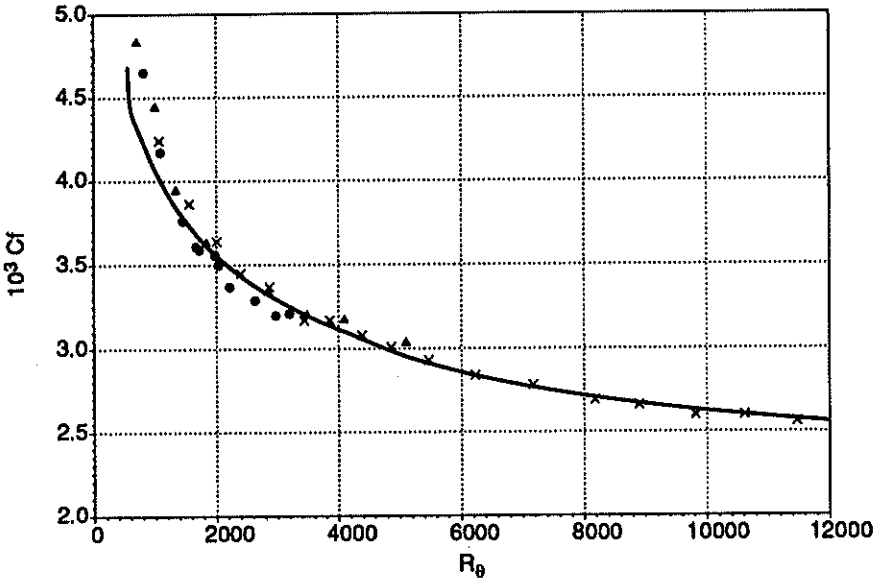

FIGURE 6. Friction coefficient versus momentum thickness Reynolds number. Solid line, present model. △, Purtell et al. (1981), ×, Weighardt and Tillman (Coles and Hirst 1968), •, Bell (Coles and Hirst 1968).

Figure 5 shows model computations and DNS data of Kim and Moin (1989) for temperature profiles in channel flow with a heat source. The Reynolds number based on friction velocity and channel half-height is 180. The computations were done at molecular Prandtl numbers of 2.0, 0.71, and 0.1, as indicated. These computations were done with a $\overline{v\theta'}$ equation, but virtually identical results were obtained by setting $Pr_t = 1.0$ and using equation (18). These figures illustrate my previous statement that the refinements to model constants did not deteriorate the results for channel flow.

Flow in flat-plate boundary layer

A boundary layer code was written to solve the model equations in Von-Mises coordinates ($\Psi - x$), with an expanding grid to allow for boundary layer growth. With the exception of σ_k and σ_ϵ as discussed above, the model was identical to that used for the channel flow computations. The computation was initialized with profiles of U, k, ε, and $\overline{v^2}$ taken from Spalart's DNS data base (Kim private communication); Spalart's profiles for $R_\theta = 670$ were used, although similar results were obtained using his $R_\theta = 300$ profiles. For heat transfer computations, the initial mean temperature profile was given the same shape as the mean velocity profile.

In figure 6, a curve of skin friction versus momentum thickness Reynolds number is compared to experimental data. The agreement is very encouraging. A more detailed comparison is given by figure 7, which shows mean velocity profiles compared

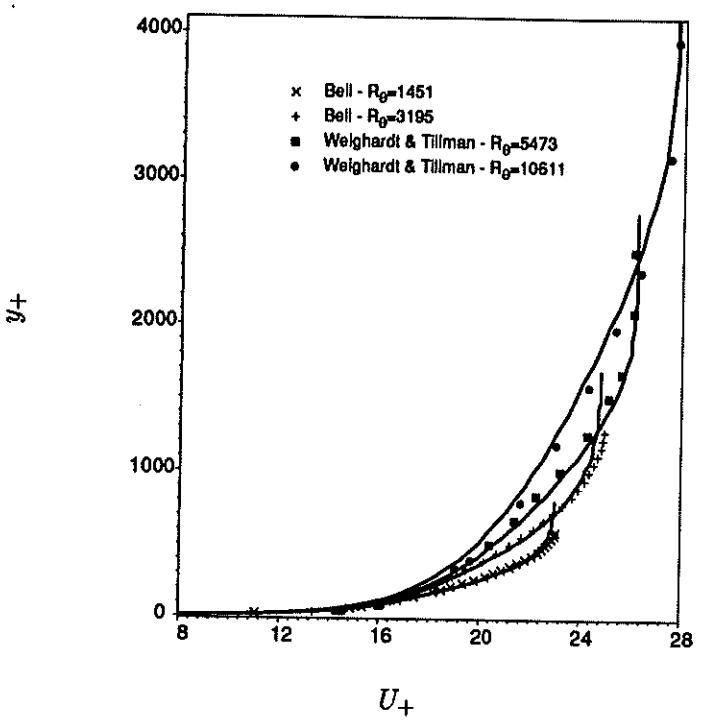

FIGURE 7. Mean velocity profiles in the range $1400 < R_\theta < 11000$. Variables are plotted in wall (+) units. Experimental data is from Coles and Hirst (1968).

to experimental data at several R_θ's in the range covered by figure 6. Again, the agreement is good. Thus, a good prediction of C_f correlates with a good prediction of the entire mean velocity profile (a similar correspondence does not prove true for the heat transfer results presented below). Although the profiles with the lower R_θ's are somewhat compacted in figure 7, expanded plots would show that the agreement to the data is as good as at higher R_θ; thus, the experimental dependence of the mean velocity on Reynolds number is reflected in the solution to the model equations. Even further detailed comparison is given by figure 8, which contains data for k and $\overline{v^2}$ transcribed from a figure in Klebanoff (1955, these data are also shown in Townsend 1976). In this case too, the agreement is satisfactory.

One objective of the near-wall model was to predict non-equilibrium boundary layers. A preliminary result in this direction is included in figure 9. This shows a computation of a boundary layer developing into an increasingly adverse pressure gradient; the pressure distribution imposed on the boundary layer is that provided in table 1 of Samuel and Joubert (1974). The primary purpose for their experiment was to provide non-equilibrium boundary layer data for model testing. An initial condition was required for the computation: this was obtained by starting with a zero pressure gradient boundary layer slightly upstream of the first measurement

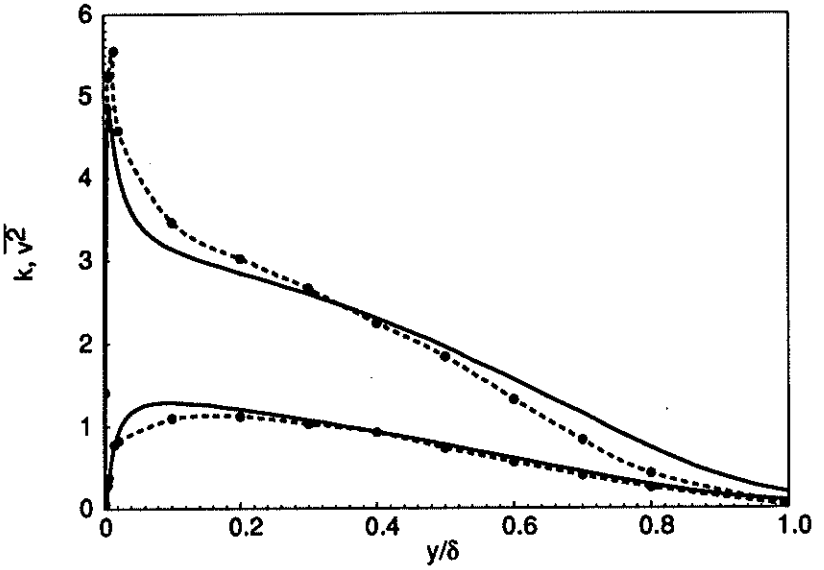

FIGURE 8. Turbulent kinetic energy (upper) and $\overline{v^2}$ compared to data transcribed from Klebanoff (1955; circles and dashed lines): $R_\theta = 7150$. y is normalized by $\delta_{.995}$ and turbulent intensities by u_*^2.

location, then subjecting it to the initial pressure gradient reported by Samuel and Joubert. The upstream distance at which the pressure gradient was imposed was determined as follows: at the first measurement location, $R_\theta = 4,992$, while $C_{f_0} = 2.79 \times 10^{-3}$; a ZPG boundary layer at this R_θ would have $C_f = 3.0 \times 10^{-3}$. It was found that the correct initial friction coefficient could be obtained by applying the pressure gradient to a ZPG boundary layer with $R_\theta = 3,200$ and allowing it to develop downstream to the position where $R_\theta = 4,992$, so this is how the computation was initialized. Figure 9 shows that quite good agreement is obtained with the experimental skin friction data. The abscissa is downstream distance in meters because this is how Samuel and Joubert report their data; for the computations, the reported value of unit Reynolds number $dRe/dx = 1.7 \times 10^6 m^{-1}$ was used to nondimensionalize both distance and the C_p gradient reported in Samuel and Joubert's table 1. They also define C_{f_0} as the friction coefficient based on an upstream reference velocity. The results in figure 9 are particularly pleasing because Rodi and Scheurer (1986) showed that the $k - \varepsilon$ model with an eddy viscosity 'damping function' was unable to predict this flow: it gave friction coefficients which were considerably too high. The present model also shows qualitative agreement with data on the evolution the k and $\overline{v^2}$ profiles and quantitative agreement with their magnitude; for brevity those results are not shown here.

Heat transfer in boundary layer

Heat transfer computations are compared to experimental data of Reynolds et

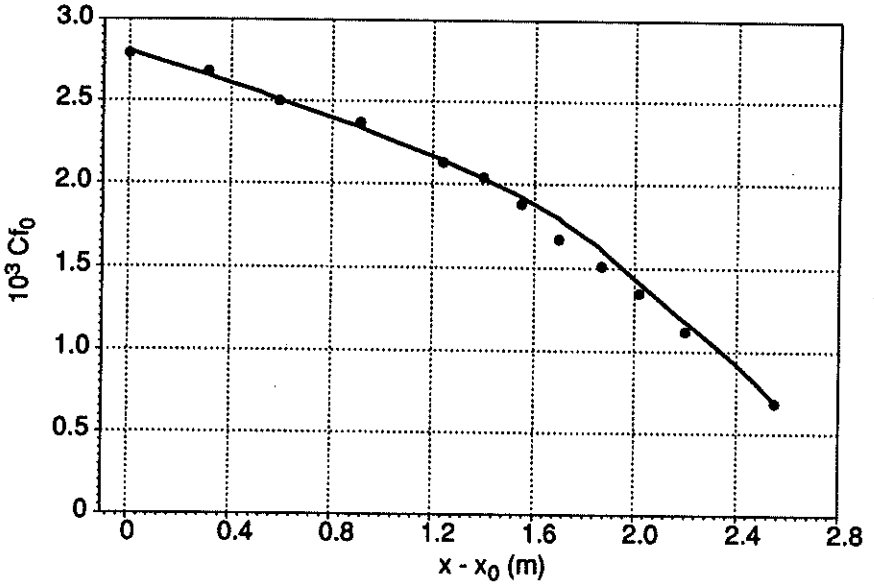

FIGURE 9. Skin friction versus downstream distance for boundary layer developing in adverse pressure gradient. Data from Samuel and Joubert (1974, table 1); solid line, present model.

al. (1958); Moffat and Kays (1984) describe these data as representative of those obtained at Stanford over the course of 25 years. Figure 10 shows Stanton number versus momentum thickness Reynolds number. The molecular Prandtl number is 0.71, corresponding to air. The calculations were done with $Pr_t = 0.9$, shown by the solid curve, and with Pr_t given by the formula

$$Pr_t = \frac{1.7}{1 + 0.4Pe_t + 0.08(e^{-5/Pe_t} - 1)Pe_t^2} \tag{19}$$

as shown by the dashed curve. In (19) Pe_t is the turbulent Peclet number ν_t/α. Formula (19) is the Prandtl number–Peclet number relation given in Moffat and Kays (1984; eq. 53—after correction of a typographical error). This formula has the property of rising steeply near the wall, reaching 1.7 at $y = 0$, and tends to 0.85 far from the wall. A steep rise of Pr_t is seen experimentally when $y_+ < 15$ (Moffat and Kays). Both of the curves in figure 10 are within the data scatter: the constant Prandtl number curve (solid) would seem to be in slightly better agreement, although the two curves are within 10% of each other.

Figure 11 shows measured and computed temperature profiles at two values of R_θ. There is a clear discrepancy between the model and data. Formula (19) was intended to improve the agreement between model and experimental temperature profiles. One sees that at the higher Reynolds number it does produce some improvement.

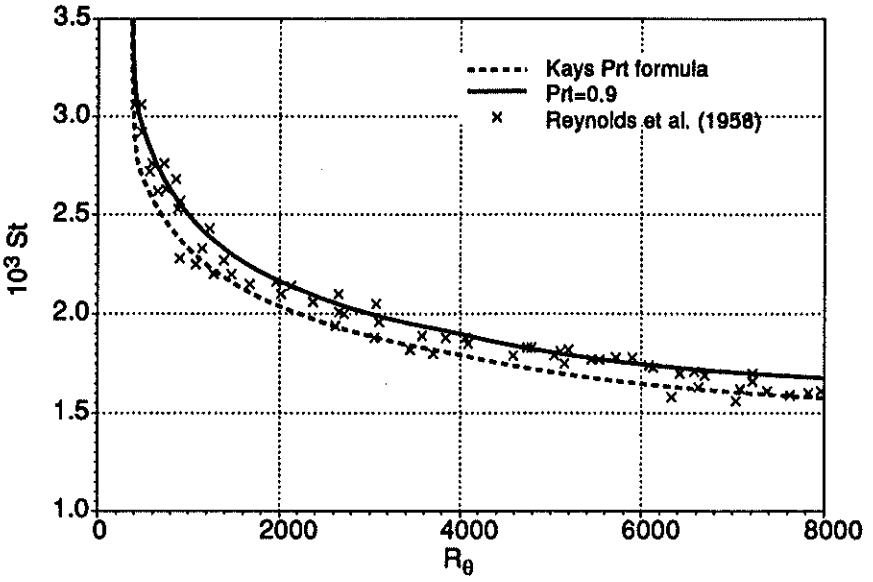

FIGURE 10. Stanton number versus momentum thickness Reynolds number. Data from Reynolds et al. (1958). Model results for two prescriptions of the turbulent Prandtl number are shown: solid line $Pr_t = 0.9$; dashed line eq. (19).

5. Future plans

The work on near wall turbulence modeling will continue into the future. Model computations of more complex boundary-layer flows will be carried out in collaboration with Dr. Ko. The application to heat transfer will be pursued further. The present type of modeling proceeds through formulation of differential equations for turbulence statistics; in the $k-\varepsilon-v$ model I have tried to introduce empiricism only through model constants, while the spatial distribution of the statistics is obtained by solving equations. The use of (19) is somewhat out of keeping with the spirit of this approach. I hope to replace such a prescribed Prandtl number relation by a $\overline{v\theta}$-equation whose solution would produce the same effect. At present, however, it is not clear how the correct near-wall behavior of $\overline{v\theta}$ should be obtained.

As I have mentioned, the work on compressed homogeneous turbulence was motivated by the work of others at CTR. I would hope to pursue some of the issues raised by this material with them. For instance, when the turbulence is not homogeneous (as near a shock wave), the kinetic energy equation contains the term

$$-\overline{u_i \partial_i p'} = \overline{p' \nabla \cdot u} - \partial_i \overline{u_i p'} . \tag{20}$$

The first term on the right side of (20) was modeled here by (12). The second term is often referred to by the seemingly inappropriate name 'pressure diffusion'. (I know of no analysis which leads to a Markovian representation for this term; indeed, it is hard to see how pressure forces become diffusive). This term is not

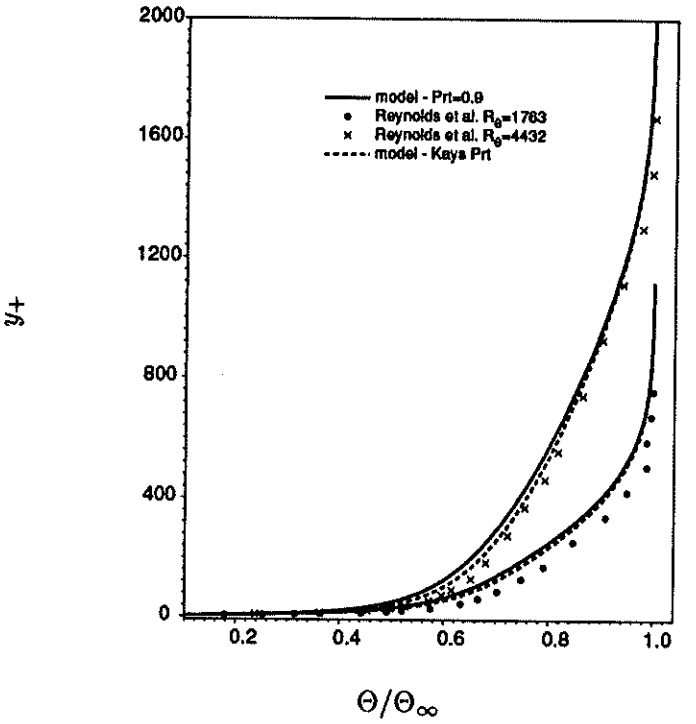

FIGURE 11. Temperature profiles compared to data from Reynolds et al. (1958) at R_θ =1763 (•) and 4432 (×). Temperature is normalized by the temperature difference across the boundary layer, and y is in + units.

peculiar to compressible turbulence, as is the first. In many flows it is negligible, but near to shocks it requires some form of modeling. It would also be desirable to extend the RDT solution to higher turbulent Mach number, where acoustic and solenoidal fluctuations interact strongly.

REFERENCES

CLAUSER, F. H. 1954 Turbulent boundary layers in adverse pressure gradients . *J. Aeronaut. Sci.* **21**, 91-108.

COLEMAN, G. N. & MANSOUR, N. N. 1991 Simulation and Modeling of Homogeneous Compressible Turbulence under Isotropic Mean Compression. 8^{th} *Symp. on Turbulent Shear Flows, Munich.*

COLES, D. E. & HIRST, E. A., EDS. 1968 *Computation of turbulent boundary layers*, AFOSR-IFP-Stanford conference.

DURBIN, P. A. 1990 Turbulence Closure Modeling near Rigid Boundaries . *CTR Ann. Res. Briefs.* 3-10; and *Theoret. Comp. Fluid Dyn.* **3**, 1-13 (1991).

DURBIN, P. A. & BELCHER, S. E. 1991 Scaling of Adverse Pressure Gradient Turbulent Boundary Layers. *CTR Manuscript 123.* to appear *J. Fluid Mech.*

DURBIN, P. A. & ZEMAN, O. 1991 Rapid Distortion Theory for Homogeneous Compressed Turbulence with Application to Modeling. *CTR Manuscript 127.*

GOLDSTEIN, M. E. 1978 Unsteady Vortical and Entropic Distortions of Potential Flows Round Arbitrary Obstacles. *J. Fluid Mech.* **89,** 433-468.

HUNT, J. C. R. 1973 A Theory of Turbulent Flow Round Two-Dimensional Bluff Bodies. *J. Fluid Mech.* **61,** 625-706.

KIM, J. & MOIN,P. 1989 Transport of Passive Scalars in a Turbulent Channel Flow. *Turbulent Shear Flows.* **6,** 85-96.

KLEBANOFF, S. 1955 Characteristics of Turbulence in a Boundary Layer with Zero Pressure Gradient. *NACA Rept.* **1247.**

LAUNDER, B. E. 1989 Second-Moment Closure: Present...and Future. *Int. J. Heat and Fluid Flow.* **10,** 282-300.

LUMLEY, J. L. 1978 Computation Modeling of Turbulent Flows. *Adv. Appl. Mech.* **18,** 126-176.

MELLOR, G. L. 1972 The large Reynolds number asymptotic theory of turbulent boundary layers. *Int. J. Engng Sci.* **10,** 851-873.

MOFFAT, R. J. & KAYS, W. M. 1984 A Review of Turbulent Boundary Layer Heat Transfer Research at Stanford 1958-1983. *Adv. in Heat Transf.* **16,** 241-365

PURTELL, L. P., KLEBANOFF, S. & BUCKLEY, F. T. 1981 Turbulent Boundary Layer at Low Reynolds Number. *Phys. Fl.* **24,** 802-811

REYNOLDS, W. C., KAYS, W. M. & KLINE, S. J. 1958 Heat Transfer in the Turbulent Incompressible Boundary Layer. *NACA memo.* **12-1-58w.**

RODI, W. & SCHEURER, G. 1986 Scrutinizing the $k - \varepsilon$ model under adverse pressure gradient conditions. *ASME J. Fluids Eng.* **108,** 174-179

SAMUEL, A. E. & JOUBERT, P. N. 1974 A Boundary Layer Developing in an Increasingly Adverse Pressure Gradient. *J. Fluid Mech.* **66,** 481-505

TOWNSEND, A. A. 1976 *The Structure of Turbulent Shear Flow* . Cambridge Univ. Press.

ZEMAN, O. 1991 Compressible Turbulence Subjected to Shear and Rapid Compression. 8^{th} *Symp. on Turbulent Shear Flows, Munich.*